Direct View at Excess Electrons in TiO$_2$ Rutile and Anatase

Martin Setvin,[1,*] Cesare Franchini,[2,†] Xianfeng Hao,[1] Michael Schmid,[1] Anderson Janotti,[3]
Merzuk Kaltak,[2] Chris G. Van de Walle,[3] Georg Kresse,[2] and Ulrike Diebold[1]

[1]*Institute of Applied Physics, Vienna University of Technology, Wiedner Hauptstrasse 8-10/134, 1040 Vienna, Austria*
[2]*Faculty of Physics and Center for Computational Materials Science, Universität Wien, Sensengasse 8/8-12, A-1090 Wien, Austria*
[3]*Materials Department, University of California, Santa Barbara, California 93106-5050, USA*

A combination of scanning tunneling microscopy and spectroscopy and density functional theory is used to characterize excess electrons in TiO$_2$ rutile and anatase, two prototypical materials with identical chemical composition but different crystal lattices. In rutile, excess electrons can localize at any lattice Ti atom, forming a small polaron, which can easily hop to neighboring sites. In contrast, electrons in anatase prefer a free-carrier state, and can only be trapped near oxygen vacancies or form shallow donor states bound to Nb dopants. The present study conclusively explains the differences between the two polymorphs and indicates that even small structural variations in the crystal lattice can lead to a very different behavior.

The behavior of charge carriers in oxides is of key importance in virtually all applications of these materials. When excess electrons are added to the conduction band of an oxide, they may either retain the free-carrier character or, still assuming a defect-free crystal, couple to lattice distortions induced by its presence (electron-phonon interaction). The latter case is usually referred to as a small or large polaron, depending on the degree of electron localization [1,2]. Polaronic effects and electron localization affect a materials' physical and chemical properties, yet it remains controversial how to model it appropriately from first principles [3,4]. Here we investigate TiO$_2$, a prototypical metal oxide. TiO$_2$ is used in catalysis [5–8], photoelectrochemical (Grätzel) solar cells, memristors [9], and as a transparent conductive oxide [10]. Two forms of TiO$_2$ are used industrially, rutile and anatase. The metastable anatase form is generally present in nanomaterials and shows better performance in energy-related applications and in optoelectronics. Even after several decades of research, a consensus on the origin of the difference between the two materials is still absent, and our aim is to resolve this issue theoretically as well as experimentally.

Stoichiometric rutile and anatase are both insulators with a ≈ 3 eV band gap. TiO$_2$ can be turned into an n-type semiconductor by adding excess electrons by various means—doping, UV irradiation, or chemical reduction. Electrons in the conduction band of TiO$_2$ compete between free-carrier and polaronic configurations. The extent to which this happens has remained highly controversial, yet strongly affects the material's transport properties and catalytic activity. The electrons can localize at Ti $3d$ orbitals, forming Ti^{3+} ions. This induces relaxations of the surrounding lattice atoms by typically 0.1 Å. The quasiparticle consisting of an electron coupled to the lattice relaxations in its immediate surrounding is called a small polaron [1]. When thermally activated, small polarons exhibit hopping mobility. If the structural deformation spreads over a large number of lattice sites the corresponding solution is categorized as a large polaron.

Here we use the following joint theoretical and experimental approach. First, we theoretically investigate the intrinsic behavior of an excess electron added to the perfect crystal, i.e., stoichiometric bulk cells of anatase and rutile. We establish that rutile allows polaron formation at any Ti site, while anatase prefers a free-carrier configuration. Next, we inspect the effect of excess electrons donated by surface oxygen vacancies (V_Os) by comparing experimental and density functional theory (DFT + U) data. We use bulk-terminated rutile (110)-(1 × 1) and anatase (101)-(1 × 1) surfaces. In rutile, the excess electrons leave the V_Os and form polarons, which can hop through the lattice. In anatase, the electrons stay trapped at the V_Os. Finally, we show that in Nb-doped anatase electrons are spatially confined by the donor potential, yet they keep the bandlike character.

For our calculations we used the VASP code [11]. On the experimental side, low-temperature scanning tunneling microscopy and spectroscopy (STM/STS) was used. Filled-states STM images reflect the spatial distribution of electrons within the band gap, and STS provides information about the electronic energy E_{EL} (see below): Either ~ 1 eV below Fermi level (E_F) typical for small polarons [5], or ~ 40 meV below E_F for delocalized, weakly bound electrons [12].

The energy balance for polaron formation in defect-free TiO$_2$ is sketched in Fig. 1(a). The formation energy, E_{POL}, is defined as the total energy difference between the polaronic and fully delocalized free-carrier solution, and results from the competition between the strain energy required to distort the lattice (E_{ST}), and the electronic energy gained by localizing the electron at a Ti site in such

a distorted lattice, E_{EL}. Polarons show a complex behavior. The electronic energy $E_{EL} = E_{POL} + E_{ST}$ is the quantity measured in photoemission spectroscopy (PES) or STS, as the lattice atoms are "frozen" within the time scale of the experimental probe [2,5,13]. For the purpose of electrical conductivity, however, activation energies are typically ~tens of meV. This is indicative of either a low barrier for hopping between neighboring polaronic configurations, or a small excitation energy from the polaronic to the free-carrier state [13].

Figure 1(b) illustrates why theoretical modeling of the polarons in TiO$_2$ and other oxides remains a challenging and controversial issue. Standard DFT always yields delocalized solutions. Electrons can be localized by applying a Hubbard U; the value of U, and thus E_{EL}, will then determine whether the polaronic solution will be stable [14–18]. The situation is equally critical with hybrid functionals, where E_{EL} depends on the amount of exact exchange incorporated in the DFT functional [4,13,19,20].

From Fig. 1(b) we infer that E_{POL} is 0.4 eV larger in rutile than anatase, and that a larger U is required to form a small polaron in anatase ($U > 5$ eV) than in rutile ($U > 3.5$ eV). We find that both materials have a similar E_{ST} (0.41 eV); the difference in E_{POL} originates from the electronic energy E_{EL}. The formation of a polaron involves the depletion of the conduction band minimum (CBM), which has a different character in the two TiO$_2$ polymorphs. Figures 1(c) and 1(d) show that the conduction band in anatase is 1 eV wider than in rutile, and the CBM lies lower in energy as a result of the formation of a strong bonding linear combination between neighboring Ti d_{xy} orbitals. Thus, a larger U is required to alter this energetically favorable configuration and to form a polaron in anatase. The associated energy gain E_{EL} is lower as compared to rutile.

The most commonly used values of U for TiO$_2$ range between 2.5 and 4.5 eV [21,22]. We calculated the U parameter entirely from first principles using the constrained random phase approximation (cRPA) [23] and obtained a value of $U^{cRPA} = 3.9$ eV for rutile and 4.1 eV for anatase. All results in the present work have been consistently determined using $U^{cRPA} = 3.9$ eV. From Fig. 1, it is clear that $U^{cRPA} = 3.9$ eV suffices to stabilize the polaron in rutile, albeit just, whereas polaron formation is clearly unfavorable in a perfect anatase lattice. In rutile the excess electron is trapped in a Ti^{3+} site, forming a small polaron; the 6 O atoms surrounding Ti^{3+} relax outward by 2%–4% of the equilibrium Ti-O bond length. In anatase, the excess electron exhibits a free-carrier "delocalized" character: the crystal remains unperturbed and the excess electron is homogeneously distributed in the crystal.

STM/STS measurements for rutile (110) and anatase (101) are compared in Fig. 2. As in previous work on rutile (110) [24,25], we take advantage of surface O vacancies (V_O) that readily form under standard preparation conditions
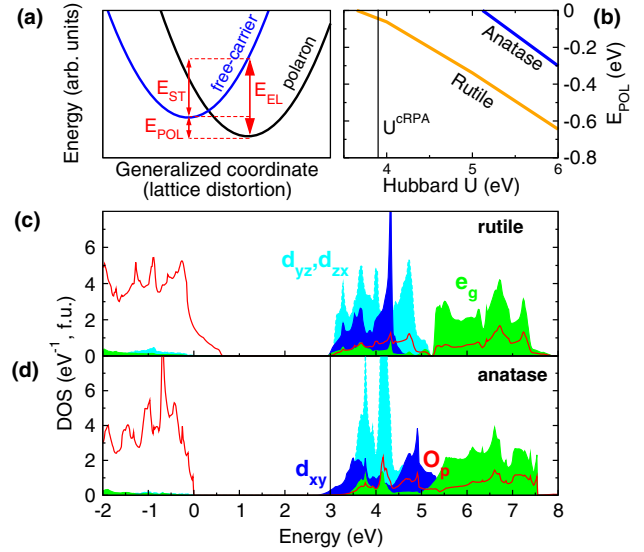

FIG. 1 (color online). Calculated polaronic stability for bulk TiO$_2$ rutile and anatase. (a) Configuration coordinate diagram showing the polaronic (E_{POL}), lattice (E_{ST}), and electronic (E_{EL}) energies as a function of lattice distortion for the polaronic and delocalized solution. (b) E_{POL} as a function of Hubbard U in bulk rutile (orange) and anatase (blue). The vertical line indicates the *ab initio* U^{cRPA}. Orbitally decomposed density of states (DOS) in rutile (c) and anatase (d), aligned with respect to the Ti core levels.

[5] to provide excess charge (donors). At anatase (101), V_Os migrate to the bulk at temperatures as low as 200 K, but surface V_Os can be created nonthermally [26]. Here subsurface V_Os were pulled to the surface using the field of the STM tip as shown in Ref. [27].

For rutile [Fig. 2(c)] the filled local density of states (LDOS) directly at the V_O is small; most of the current comes from the rows of five-coordinated surface Ti$_{5c}$ atoms. This is even more apparent when scanning at very close tip-sample distances [see lower part of the image in Fig. 2(c), and the Supplemental Material [28] for details]. In contrast, the electrons stay at the vacancy at anatase [Fig. 2(d)] as suggested by the vanishing LDOS at the rest of the surface.

Point tunneling spectra were measured at various distances from the surface V_Os on rutile and anatase; see Figs. 2(g) and 2(h). The STS peak positions agree well with photoemission spectra taken from our samples as well as other published data [5,29]. The CBM is located just above E_F, as expected for reduced TiO$_2$; band bending does not play a significant role. In STS on rutile, the polaronic bandgap state is found 0.7 ± 0.1 eV below E_F; again, the spectra are very similar when taken either directly at the vacancy or at the Ti$_{5c}$ rows. On anatase, the gap state is found at 1.0 ± 0.1 eV below the Fermi level [29], and it is strictly localized at the vacancy. When the point spectrum is measured away from the V_Os at anatase (101), this gap state is not detected.
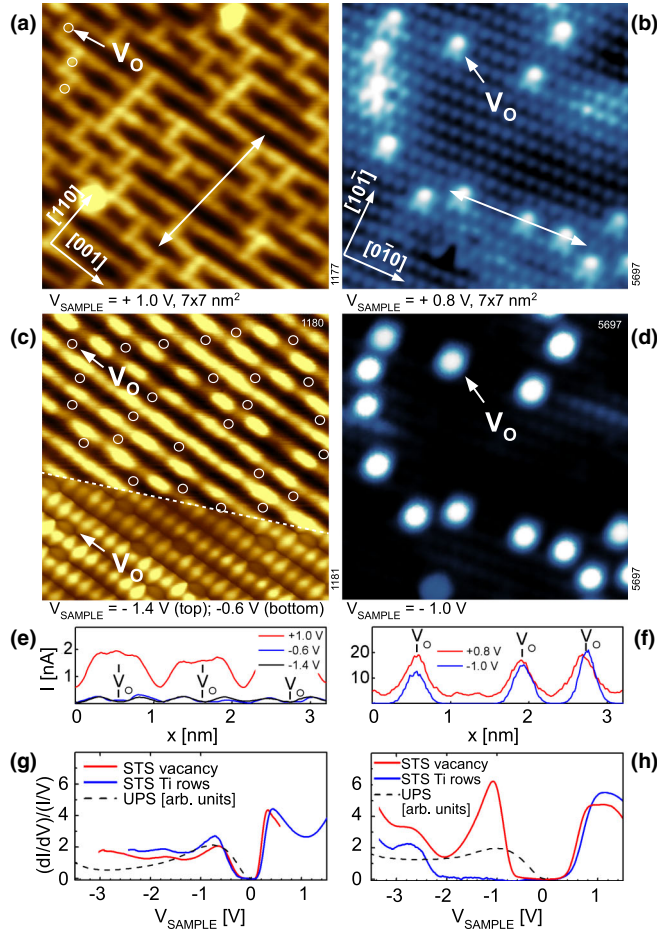
FIG. 2 (color online). Local electronic structure of rutile (110) (left) and anatase (101) (right) surfaces doped by surface oxygen vacancies. Constant-height scanning tunneling microscopy images of (a),(b) empty states and (c),(d) filled states of the same areas. V_O marks surface oxygen vacancies; they are also marked with circles in (c). (e),(f) Line profiles along the lines in (a) and (b), respectively. STS measured above V_O and above regular fivefold coordinated Ti_{5c} surface atoms of (g) rutile and (h) anatase. Photoemission spectra ($h\nu = 120$ eV, dashed lines) are included for comparison. Rutile at $T = 78$ K, anatase at $T = 6$ K.

FIG. 3 (color online). Surface calculations of excess electrons in rutile (110) and anatase (101) donated by a surface V_O. In rutile, small polarons can assume many energetically almost equivalent positions. (a) Configurations with two subsurface polarons P_{sub} (top) and one P_{sub} plus one surface polaron P_{surf} (bottom). (b) The only stable configuration at the anatase surface, with both excess electrons bound to the surface V_O. (c) Polaron dynamics in rutile (orange) and anatase (blue) and corresponding statistical analysis for rutile. The small polarons stay mostly in the subsurface $(S - 1)$ below the vacancy and at surface (S) Ti_{5c} sites. (d)–(g) Calculated STM images for empty (d),(e) and filled (f),(g) states in rutile (left, the three most frequent polaronic configurations according to the MD analysis) and anatase (right, the electron is always trapped at the surface V_O).

Previous calculations on rutile showed that many polaronic configurations have almost identical total energies [Fig. 3(a)] [16,30,31]. In our first principles molecular dynamics (MD) calculations, closely following Ref. [16], the polarons also hop rapidly among lattice Ti sites [Fig. 3(c)]. Mostly (~75% of the time) they stay in the first subsurface layer; occasionally (~25%) they move to the surface Ti_{5c} sites [16]. Calculated empty- and filled-states images for three such configurations are shown in Figs. 3(d) and 3(f). The polaron position does not affect the empty-states image, whereas it is apparent when imaging filled states [crosses in Figs. 3(f) and 3(g)]. In STM on rutile at $T = 78$ K, we measure a weighted average of the polaronic configurations, where both the surface and the
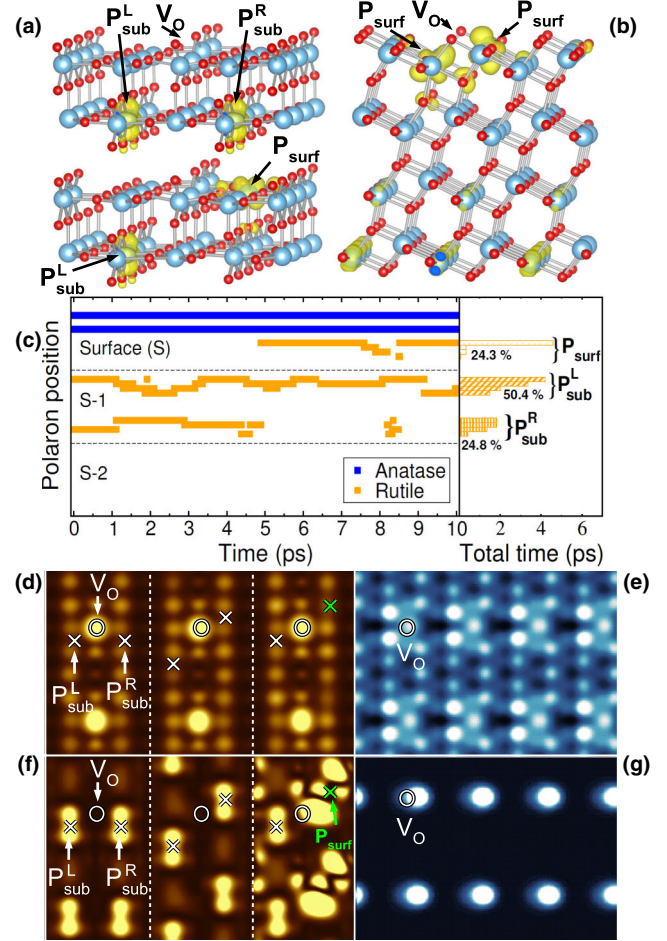
subsurface small polarons contribute. Below $T = 20$ K, we observed the complete absence of conductivity suggesting that the polarons freeze in.

In stark contrast to rutile, however, a surface V_O on anatase gives rise to immobile electrons pinned at Ti sites just at the V_O [21] with a high E_{EL} of ~1 eV [Figs. 3(b) and 3(c)]; these electrons are observed in filled-states STM [compare Figs. 2(d) and 3(g)]. In total-energy calculations any attempt to move the electron to a different bulk Ti lattice site resulted in an unstable, high-energy configuration.
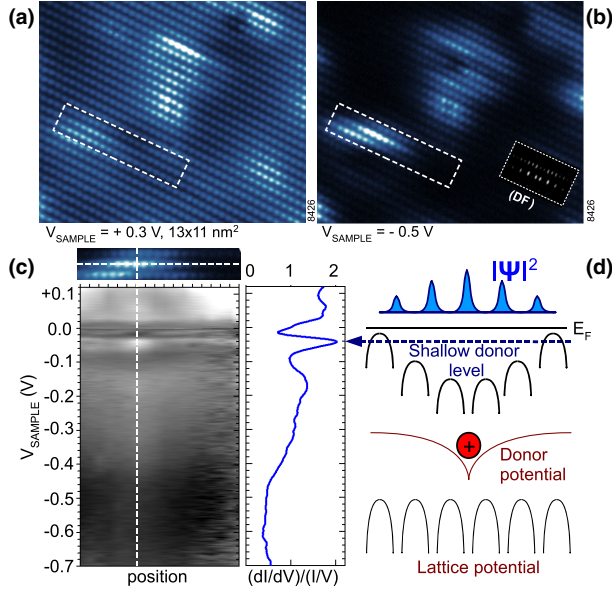
FIG. 4 (color online). Shallow donor state at Nb-doped anatase (101). (a) Empty and (b) filled states STM images taken at $T = 6$ K (constant height). The bright areas are in the vicinity to subsurface dopants. The inset "DFT" in (b) shows a calculated STM image of the shallow donor state. The electron wave function is more extended along the [010] (12–25 Å), then along the [101] (4–8 Å) direction. (c) Spatially resolved plot of $(dI/dV)/(I/V)$ along the blue dashed line. (Note the different energy scale as compared to Fig. 2.) (d) Model of the shallow donor state.

The electron localization close to the anatase surface V_O is facilitated by high local structural flexibility of the lattice near the vacancy, decreasing the strain energy E_{ST}.

When electrons are introduced via a dopant that modifies the lattice structure only slightly (see the Supplemental Material [28]), polaron formation remains favorable in rutile, whereas spatially more extended solutions are preferred in anatase. This is reflected in the 4 orders of magnitude larger conductivity of Nb-doped anatase compared to Nb-doped rutile: anatase exhibits metal-like temperature dependence of the conductivity, whereas rutile retains a semiconductor-like character [10,32]. Our DFT $+$ U calculations suggest that the higher conductivity in Nb-doped anatase is due to the absence of localized small polarons, whereas in rutile—with the same U—small polarons are formed. The STM results are again entirely consistent with this prediction. In an anatase sample doped with $\sim$1% Nb [27], fairly extended bright regions in the STM images with a measurable density of states below E_F (Fig. 4) are visible. The Nb dopants were distributed unevenly in our sample. Figure 4 shows a region with low concentration. Spatially resolved STS [Fig. 4(c)] images reveal a peak at (-40 ± 10) meV and the absence of any gap state at -1 eV. The bright regions shown in Figs. 4(a) and 4(b) are stable in time and do not migrate within a temperature range from 6 to 78 K, suggesting that the

electron is stabilized at the positively charged subsurface donor, most likely Nb. Figure 4(d) shows a simple model. The ionized donor creates a quantum well, where the electron occupies a single energy level. The electron wave function is spread over several unit cells around the donor, and is modulated by the periodic potential of the crystal lattice; a calculated STM image of a slab with a Nb impurity [inset of Fig. 4(b)] agrees well with the experiment. For details see the Supplement Material [28]. In recent ARPES measurements [12] a similar peak at (40 ± 10) meV below E_F was attributed to a "large polaron." The distinction between a shallow, delocalized donor level and a large polaron is subtle. DFT $+ U$ calculations reproduce the measured STM image only when lattice relaxations (polaronic effects) are taken into account. In STM images the density distribution has an anisotropic shape, with spatial extensions of $\Delta r[010] = 12$–25 Å and $\Delta r[10\bar{1}] = 4$–8 Å. This agrees well with Fröhlich's model for large polarons [1], from which we obtain $\Delta r[010] = 19.0$, and $\Delta r[10\bar{1}] = 3.5$ Å related to the anisotropy of the screening and effective masses (see the Supplemental Material [28]). Thus, this state is similar to a large polaron, but cannot move through the crystal like a true polaron.

Our study illustrates the basic principles of excess electron behavior in the model oxide TiO_2. The different stacking of octahedrally coordinated Ti in the two polymorphs, and the resulting subtle differences in the electronic structure around the CBM, provide for a higher energy gain upon small polaron formation in rutile than in anatase. Filled states STM clearly shows the various cases: Small polarons that readily hop in rutile, electrons trapped at surface V_Os in anatase, and spatially extended shallow donor states in Nb-doped anatase. STS also shows distinct signatures, with an apparent deep ($\sim$eV) polaronic state for rutile, yet a much shallower state (40 meV) at dopants of anatase. The latter shows spectroscopic similarities with recent ARPES results [12] and its lateral extension is well described by Fröhlich's theory for large polarons. These experimental results prove electron localization for rutile and delocalization for anatase *surfaces*. Recent EPR data [3] indicate the same behavior in the *bulk* of these materials, in agreement with the calculations in Fig. 1(b).

Polarons are central to the often exotic behavior of oxides [33] as well as their technological applications. In the specific case of TiO_2, anatase is used as an electrode in photoelectrochemical solar cells. Bandlike charge transport and the lack of small polaron formation is the key requirement for increasing the cell efficiency. On the other hand, the formation of small polarons in rutile is an asset in catalysis, as the polaron formation is more favorable at surfaces than in the bulk, facilitating an efficient charge transfer to catalyzed species [6]. In mixtures of the two TiO_2 phases, anatase provides a good electron conductor that transports charge carriers to the interface with rutile, where they are trapped [34].

---

[*] setvin@iap.tuwien.ac.at
[†] cesare.franchini@univie.ac.at
[1] H. Fröhlich, Adv. Phys. **3,** 325 (1954).
[2] I. G. Austin and N. F. Mott, Adv. Phys. **50,** 757 (2001).
[3] M. Chiesa, M. C. Paganini, S. Livraghi, and E. Giamello, Phys. Chem. Chem. Phys. **15,** 9435 (2013).
[4] C. Di Valentin, G. Pacchioni, and A. Selloni, J. Phys. Chem. C **113,** 20 543 (2009).
[5] U. Diebold, Surf. Sci. Rep. **48,** 53 (2003).
[6] M. A. Henderson, Surf. Sci. Rep. **66,** 185 (2011).
[7] A. Linsebigler, G. Lu, and J. R. Yates, Chem. Rev. **95,** 735 (1995).
[8] Z. Dohnalek, I. Lyubinetsky, and R. Rousseau, Prog. Surf. Sci. **85,** 161 (2010).
[9] K. Szot, M. Rogala, W. Speier, Z. Klusek, A. Besmehn, and R. Waser, Nanotechnology **22,** 254001 (2011).
[10] S. X. Zhang, D. C. Kundaliya, W. Yu, S. Dhar, S. Y. Young, L. G. Salamanca-Riba, S. B. Ogale, R. D. Vispute, and T. Venkatesan, J. Appl. Phys. **102,** 013701 (2007).
[11] G. Kresse and J. Furthmüller, Comput. Mater. Sci. **6,** 15 (1996).
[12] S. Moser et al., Phys. Rev. Lett. **110,** 196403 (2013).
[13] A. Janotti, C. Franchini, J. B. Varley, G. Kresse, and C. G. Van de Valle, Phys. Status Solidi RRL **7,** 199 (2013).
[14] N. A. Deskins and M. Dupuis, Phys. Rev. B **75,** 195212 (2007).
[15] Z. Hu and H. Metiu, J. Phys. Chem. C **115,** 5841 (2011).
[16] P. M. Kowalski, M. F. Camellone, N. N. Nair, B. Meyer, and D. Marx, Phys. Rev. Lett. **105,** 146405 (2010).

[17] L. Chiodo, J. M. García-Lastra, A. Iacomino, S. Ossicini, J. Zhao, H. Petek, and A. Rubio, Phys. Rev. B **82,** 045207 (2010).
[18] B. J. Morgan and G. W. Watson, Surf. Sci. **601,** 5034 (2007).
[19] T. Shibuya, K. Yasuoka, S. Mirbt, and B. Sanyal, J. Phys. Condens. Matter **24,** 435504 (2012).
[20] P. Deak, B. Aradi, and T. Frauenheim, Phys. Rev. B **86,** 195206 (2012).
[21] H. Cheng and A. Selloni, J. Chem. Phys. **131,** 054703 (2009).
[22] E. Finazzi, C. Di Valentin, G. Pacchioni, and A. Selloni, J. Chem. Phys. **129,** 154113 (2008).
[23] F. Aryasetiawan, K. Karlsson, O. Jepsen, and U. Schönberger, Phys. Rev. B **74,** 125106 (2006).
[24] T. Minato et al., J. Chem. Phys. **130,** 124502 (2009).
[25] A. C. Papageorgiou, N. S. Beglitis, C. L. Pang, G. Teobaldi, G. Cabailh, Q. Chen, A. J. Fisher, W. A. Hofer, and G. Thornton, Proc. Natl. Acad. Sci. U.S.A. **107,** 2391 (2010).
[26] P. Scheiber, M. Fidler, O. Dulub, M. Schmid, U. Diebold, W. Hou, U. Aschauer, and A. Selloni, Phys. Rev. Lett. **109,** 136103 (2012).
[27] M. Setvin, U. Aschauer, P. Scheiber, Y.-F. Li, W. Hou, M. Schmid, A. Selloni, and U. Diebold, Science **341,** 988 (2013).
[28] See Supplemental Material at http://link.aps.org/supplemental/10.1103/PhysRevLett.113.086402 for details.
[29] A. G. Thomas et al., Phys. Rev. B **75,** 035105 (2007).
[30] N. A. Deskins, R. Rousseau, and M. Dupuis, J. Phys. Chem. C **115,** 7562 (2011).
[31] P. Krüger et al., Phys. Rev. Lett. **100,** 055501 (2008).
[32] D. Morris, Y. Dou, J. Rebane, C. Mitchell, R. Egdell, D. Law, A. Vittadini, and M. Casarin, Phys. Rev. B **61,** 13 445 (2000).
[33] E. K. H. Salje, A. S. Alexandrov, and W. Y. Liang, *Polarons and Bipolarons in High-T_c Superconductivity and Related Materials* (Cambridge University Press, Cambridge, England, 1995).
[34] D. O. Scanlon et al., Nat. Mater. **12,** 798 (2013).